Fluorescence Spectroscopic Properties of Nitro-Substituted Diphenylpolyenes: Effects of Intramolecular Planarization and Intermolecular Interactions in Crystals

Yoriko Sonoda,*,† Seiji Tsuzuki,‡ Midori Goto,§ Norimitsu Tohnai,|| and Masaru Yoshida†

Nanotechnology Research Institute and Technical Center, National Institute of Advanced Industrial Science and Technology (AIST), Higashi 1-1-1, Tsukuba, Ibaraki 305-8565, Japan, Research Institute of Computational Sciences, AIST, Umezono 1-1, Tsukuba, Ibaraki 305-8568, Japan, and Department of Material and Life Science, Graduate School of Engineering, Osaka University, 2-1, Yamadaoka, Suita, Osaka 565-0871, Japan

Received: August 3, 2009; Revised Manuscript Received: October 25, 2009

The steady-state absorption and fluorescence properties of (*E*,*E*,*E*)-1,6-diaryl-1,3,5-hexatrienes (**2**, aryl = 2-nitrophenyl; **3**, aryl = 3-nitrophenyl; **4**, aryl = 4-nitrophenyl) have been investigated in solution and in the crystalline state. The solid-state absorption spectra of **2**−**4** shifted to longer wavelengths than those in solution. A combination of theoretical calculations and single-crystal X-ray structure analyses shows considerable planarization of molecules in the solid state, which is mainly responsible for the spectral red shifts. The effects of intermolecular interactions on the absorption spectra appeared to be relatively small in these crystals. This is consistent with the monomeric origin of the solid-state emission. Molecule **2** was nonfluorescent in all solvents studied, probably due to the efficient nonradiative deactivation from ionic species produced by excited-state intramolecular proton transfer (ESIPT) along the C−H···O-type hydrogen bonds. The fluorescence of **3**, observed only in medium polar solvents, originated from an intramolecular charge transfer (ICT*) state, while that of **4** derived from locally excited (LE*) and/or ICT* states depending on the solvent polarity. All three molecules exhibited LE* fluorescence in the solid state. No observation of ICT* emission in crystals strongly suggests the twisted geometries for ICT* (TICT) of **3** and **4** in solution. The measurable fluorescence from crystal **2** can be attributed to the restricted torsional motions in the solid excited state.

Introduction

Light absorption and fluorescence emission of organic dyes in the solid state is a fundamental issue not only in molecular science but also in material science.[1] In particular, fluorescence emission from organic solids is of great interest due to their potential use as photoactive materials such as light-emitting diodes (LEDs),[2−6] solid-state lasers,[7,8] and light-emitting electrochemical cells.[9]

Despite the extensive studies, however, understanding and even more predicting the absorption and fluorescence spectroscopic behavior of organic solids is still difficult.[10] The relationship between molecular structure and spectroscopic properties is well-known in solution, while in the solid state, the structure−property relationship is much more complicated. The spectra in the solid state are in general red-shifted compared to those in solution, and the shifts can mainly be attributed to molecular planarization and intermolecular interactions in the solid state.[11−14] Flexible molecules in solution are often frozen in more planar conformations in the solid state. The molecular planarization leads directly to the extended delocalization of the π-electronic system. The intermolecular interactions, which are closely related to the molecular arrangements in the solid state, can also affect the energy levels of the electronic systems of the molecules. For better understanding of the absorption and fluorescence behavior of organic molecules in the solid state, systematic studies on the effects of intramolecular planarization and intermolecular interactions on the spectroscopic properties are required.

CHART 1: Chemical Structures and Atom Numberings of 1−4

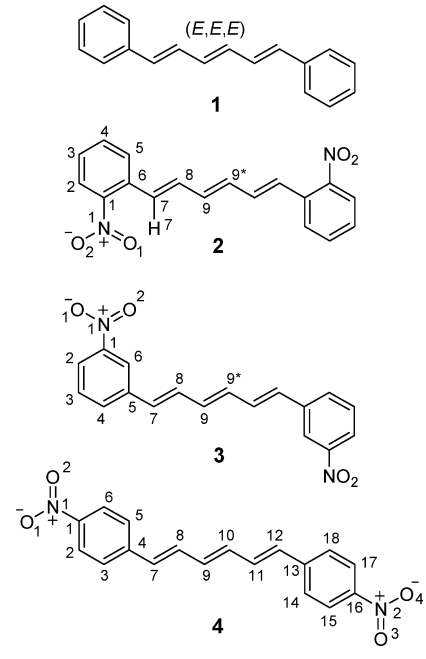

(*E*,*E*,*E*)-1,6-Diphenyl-1,3,5-hexatriene (DPH) (**1**, Chart 1) is a highly fluorescent molecule with a one-dimensional polyenic structure and is commercially available as a fluorescence probe in biological membrane studies. The emission properties of **1**

* Corresponding author: fax, +81-29-861-4673; e-mail, y.sonoda@aist.go.jp.
† Nanotechnology Research Institute.
‡ Research Institute of Computational Sciences.
§ Technical Center.
|| Osaka University.

10.1021/jp907441p
Published on Web 11/23/2009

in solution have long attracted much attention because of its dual fluorescence from the first two singlet excited states, S_1 and S_2.[15,16] As for the emission properties in the solid state, on the other hand, much remains to be clarified. We showed that *p*,*p*′-disubstituted DPHs exhibited measurable fluorescence also in the solid state.[17] The fluorescence maximum (λ_f) moved to longer wavelengths as the strength of electron-withdrawing (EW) or electron-donating (ED) nature of substituents increased. Our recent studies further show that, in a series of donor−acceptor *p*-(*n*-alkoxy)-*p*′-nitro-substituted[18] and ring-fluorinated[19] DPHs, the crystal packing patterns strongly affect not only λ_f but also the origin of the solid-state fluorescence (e.g., monomeric, excimeric, and ground-state aggregated species), reflecting the magnitude of the intermolecular interactions in crystals.

We previously investigated the photophysical properties of nitro-substituted DPH (**4**, Chart 1) in solution.[20] Aromatic nitro compounds are in general only weakly fluorescent or completely nonfluorescent in solution, due to the efficient nonradiative decay (NRD) processes such as singlet−triplet intersystem crossing (ISC) and internal conversion (IC).[21−27] In addition, they often undergo intra- and intermolecular hydrogen abstraction, resulting in rapid photodecomposition.[27−29] Despite these general tendencies of nitroaromatics, **4** exhibited relatively strong fluorescence (quantum yield $\phi_f = 0.61$ in dichloromethane (DCM)) and was proven to be photochemically very stable in solution. The strongly red-shifted fluorescence of **4** in polar solvents was assigned to the emission from an intramolecular charge transfer state (ICT*), for which the twisting of $C_6H_4(Ar)-NO_2$ single bond was strongly suggested. If this is the case, then the solid-state fluorescence behavior of **4** can differ significantly from that in solution, as a result of molecular planarization along with possible intermolecular interactions involving the nitro groups in crystals.

In this study, the absorption and fluorescence properties of *o*,*o*′-, *m*,*m*′-, and *p*,*p*′-dinitro-substituted DPHs (**2**, **3**, and **4**, respectively, in Chart 1) were investigated in solution and in the crystalline state. These structural isomers are expected to have different molecular planarity and different packing patterns in crystals, depending on the position of the nitro substituent on the benzene ring. We performed ab initio and DFT calculations and single-crystal X-ray analyses to clarify the structures of molecules in solution and in the solid state. Crystals **2**−**4** were all photostable. No *Z*−*E* isomerization or [2 + 2] cycloaddition was observed in these crystals.

Experimental Section

Materials. Compound **1** was purchased from Wako (scintillation grade) and used without further purification. Compounds **2**−**4** were synthesized from nitrobenzaldehydes (TCI) and (*E*)-2-butene-1,4-bis(triphenylphosphonium chloride) (TCI) by procedures similar to those described in the literature.[30] Elemental analyses were performed using a CE instruments EA-1100. IR spectra were recorded on a Mattson Infinity Gold FT-IR spectrometer. ^{1}H and ^{13}C NMR spectra were recorded on a Varian Gemini-300 BB spectrometer (300.1 and 75.5 MHz, respectively) with tetramethylsilane (TMS) as internal reference. All solvents used in the measurements of absorption and fluorescence spectra were of spectroscopic grade (Dojin).

***(E,E,E)*-1,6-Di(2-nitrophenyl)-1,3,5-hexatriene (2).** The crude product of the reaction between 2-nitrobenzaldehyde and the phosphonium salt was recrystallized three times from toluene (Tol) to give single crystals of **2** suitable for X-ray analysis. The purity was checked by HPLC. mp 230−231 °C (lit.[31] 230−231.5 °C; lit.[30] 232−233 °C). Anal. Calcd for $C_{18}H_{14}N_2O_4$: C, 67.07; H, 4.38; N, 8.69. Found: C, 67.14; H, 4.29; N, 8.59. ν_{max} (KBr) 1602, 1567, 1510, 1474, 1441, 1338, 1301, 1277, 1007, 993, 956, 781, 741, 695, and 625 cm^{-1}. ^{1}H NMR ($CDCl_3$) δ 7.93 (2H, d, *J* 8.1, arom.), 7.71 (2H, d, *J* 7.8, arom.), 7.58 (2H, apparently (app.) t, *J* 7.6, arom.), 7.38 (2H, app. t, *J* 7.7, arom.), 7.16 (2H, d, *J* 15.3, triene), 6.91 (2H, app. ddd, *J* 15.1, 6.9 and 3.0, triene), 6.65 (2H, app. dd, *J* 7.0 and 2.9, triene). ^{13}C NMR ($CDCl_3$) δ 147.9, 135.2, 133.6, 132.9, 132.4, 128.1, 128.0, 127.7, and 124.8. UV−vis λ_{max} (acetonitrile (AN)) 327 nm ($\epsilon = 35000$ M^{-1} cm^{-1}), 373 nm ($\epsilon = 27900$ M^{-1} cm^{-1}); λ_{max} (Tol) 331 nm ($\epsilon = 27100$ M^{-1} cm^{-1}), 385 nm ($\epsilon = 27800$ M^{-1} cm^{-1}).

***(E,E,E)*-1,6-Di(3-nitrophenyl)-1,3,5-hexatriene (3).** The crude product of the reaction between 3-nitrobenzaldehyde and the salt contained a large amount of *Z* isomers as shown by ^{1}H NMR and UV−vis spectra. To induce *Z*-to-*E* isomerization, the product was irradiated in DCM with Pyrex-filtered light at room temperature in air. The solvent was evaporated and the resulting yellow solid (predominantly *E*,*E*,*E*) was recrystallized from Tol to give single crystals of **3** suitable for X-ray analysis. The purity was checked by HPLC. mp 234−236 °C (lit.[30] 165−166 °C). Anal. Calcd for $C_{18}H_{14}N_2O_4$: C, 67.07; H, 4.38; N, 8.69. Found: C, 67.19; H, 4.37; N, 8.37. ν_{max} (KBr) 1572, 1531, 1472, 1439, 1355, 1281, 1098, 1073, 1018, 995, 892, 828, 806, 735, 673, and 624 cm^{-1}. ^{1}H NMR ($CDCl_3$) δ 8.28−8.29 (2H, m, arom.), 8.06−8.10 (2H, m, arom.), 7.71 (2H, d, *J* 7.9, arom.), 7.50 (2H, app. t, *J* 8.0, arom.), 7.02 (2H, app. ddd, *J* 15.4, 7.0 and 3.0, triene), 6.69 (2H, d, *J* 15.5, triene), 6.62 (2H, app. dd, *J* 7.1 and 3.1, triene). ^{13}C NMR ($CDCl_3$) δ 148.8, 136.6, 134.5, 132.2, 131.5, 131.0, 129.6, 122.1, and 120.8. UV−vis λ_{max} (AN) 352 nm ($\epsilon = 68000$ M^{-1} cm^{-1}); λ_{max} (Tol) 360 nm ($\epsilon = 57700$ M^{-1} cm^{-1}).

It should be noted that the melting point of our crystalline sample was higher by 70 °C than the value reported in the literature.[30] This is probably because the literature value was for the sample containing *Z* isomer(s).

***(E,E,E)*-1,6-Di(4-nitrophenyl)-1,3,5-hexatriene (4).** The crude product of the reaction between 4-nitrobenzaldehyde and the salt was recrystallized from Tol. The recrystallized sample, which was unsuitable for X-ray analysis, was dissolved in AN. Single crystals of **4** suitable for X-ray analysis were obtained by very slow evaporation of the AN solvent at room temperature in the dark. The purity was checked by HPLC. mp 240−241 °C (lit.[32] 195−197 °C, lit.[30] 218−219 °C, lit.[31] 229−231 °C). Anal. Calcd for $C_{18}H_{14}N_2O_4$: C, 67.07; H, 4.38; N, 8.69. Found: C, 67.04; H, 4.24; N, 8.66. ν_{max} (KBr) 1588, 1509, 1335, 1178, 1108, 994, 870, 833, 747, and 690 cm^{-1}. ^{13}C NMR ($CDCl_3$) δ 146.8, 143.4, 135.3, 132.9, 131.7, 126.9, and 124.2. ^{1}H NMR data were reported previously.[20] UV−vis λ_{max} (AN) 410 nm ($\epsilon = 76400$ M^{-1} cm^{-1}); λ_{max} (Tol) 410 nm ($\epsilon = 75700$ M^{-1} cm^{-1}).

For **4**, some different melting point values are reported in the literature. We found that the melting point of the sample obtained by simple recrystallization from Tol was 228−229 °C, whereas the single crystals obtained as above had mp 240−241 °C.

Photostability of 2−4. Although **2** was photostable in the solid state, it was decomposed on prolonged irradiation in solution, as shown by HPLC and UV−vis absorption spectra. The fluorescence spectra in solution were therefore recorded by minimum exposure to light to avoid any photoreactions[30] during the measurements.

Compounds **3** and **4** were photostable in solution and in the solid state. No *Z*−*E* photoisomerization from the *E*,*E*,*E* isomers was observed at least in DCM or Tol.

TABLE 1: Absorption and Fluorescence Data of 2 and 3 in Solution

	2[a]	3				
solvent	λ_a (nm)	λ_a (nm)	λ_f (nm)	ΔE_{ss} (cm^{-1})	ϕ_f	τ_s (ns)
methylcyclohexane	375, 328	373, 355, 340		nonfluorescent		
carbon tetrachloride	380, 331	379, 358, 342	482	7186	0.00042	0.72
toluene	385, 331	379, 360, 346	513	8285	0.0068	1.1
1,4-dioxane	381, 331	377, 357, 343	547	9729	0.011	1.7
tetrahydrofuran	380, 331	377, 357, 343	574	10589	0.0052	1.3
chloroform	385, 328	378, 358, 343		nonfluorescent		
dichloromethane	384, 328	377, 357, 342		nonfluorescent		
acetone	375, 330	374, 354, 338		nonfluorescent		
N,*N*-dimethylformamide	381, 333	378, 359, 344		nonfluorescent		
acetonitrile	373, 327	371, 352, 338		nonfluorescent		
methanol	372, 328	370, 352, 338		nonfluorescent		

[a] Nonfluorescent in all solvents studied.

Measurements of Absorption Spectra. Absorption spectra in solution were measured in air at room temperature using a Shimadzu UV-3150 spectrometer. All solutions were highly diluted ((1.0−3.5) × 10^{-5} M). Absorption spectra in the solid state were obtained by Kubelka−Munk conversion of diffuse reflectance spectra. The reflectance spectra were recorded on a Jasco V-560 spectrometer equipped with an integrating sphere accessory (model ISV-469). The sample solids were placed between quartz plates (40 × 10 mm^2).

Measurements of Fluorescence and Fluorescence Excitation Spectra, Fluorescence Quantum Yields, and Lifetimes. The corrected fluorescence and fluorescence excitation spectra in solution and in the solid state were measured at room temperature in air using a SPEX Fluorolog-3 spectrometer.

For the fluorescence measurements in solution, the excitation wavelengths were set at 330 and 380 nm for **2**, 355 nm for **3**, and 400 nm for **4**, unless otherwise noted. Concentration of the sample solutions was (1.0−3.5) × 10^{-6} M. Values of ϕ_f in solution were determined using a solution of quinine sulfate in 1 N H_2SO_4 as a standard (ϕ_f = 0.546).[33] For **4**, we measured the fluorescence data in some selected solvents under air-saturated conditions to find that they were practically identical with those measured under degassed conditions which we reported previously.[20]

Fluorescence and excitation spectra of the crystalline samples were recorded using the front face geometry. The sample crystals were placed between quartz plates (40 × 10 mm^2) on the sample holder. For all compounds, the excitation and emission wavelengths were set at 420 and 600 nm, respectively. The measurements of the solid-state ϕ_f were performed at Osaka University by using a Jasco FP-6500 spectrofluorometer with a fluorescence integrate sphere unit (model ISF-513). The sample crystals were encapsulated in a quartz cell (30 × 30 × 0.3 mm^3) under deoxygenated conditions. The excitation wavelength was 350 nm.

Fluorescence decay curves of **3** in solution and those of **2**−**4** in the solid state were obtained by the time-correlated single-photon counting (TCSPC) method, using a HORIBA NAES 700 equipped with a subnanosecond nitrogen laser system (excitation wavelength = 337 nm). The monitor wavelengths were set at λ_f as shown in Tables 1 and 6.

For the solid-state absorption and fluorescence measurements, the samples were not ground to a powder in all cases.

Single Crystal X-ray Structure Analyses. The single crystal X-ray diffraction measurements of **2** and **3** were performed at 183 K using a Bruker SMART CCD area-detector diffractometer with graphite monochromated Mo Kα radiation (λ = 0.71073 Å). Data collection and reduction and empirical absorption correction were carried out using SMART (Bruker2001), SAINTPLUS (2001), and SADABS (2001).[34] The structure was solved by direct methods using SIR92[35] and refined by full matrix least squares on F^2 with SHELXTL.[36] The non-hydrogen atoms were refined anisotropically. Hydrogen atoms were placed in geometrically calculated positions and refining a riding model.

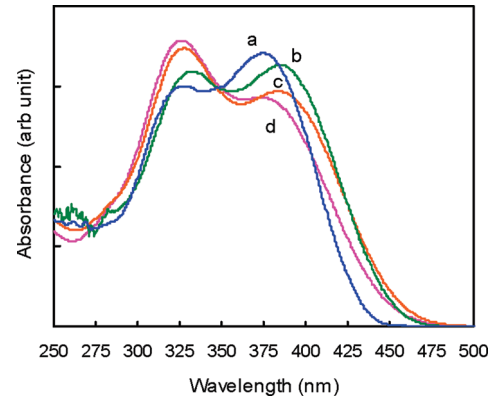

Figure 1. Absorption spectra of **2** in (a) methylcyclohexane, (b) toluene, (c) dichloromethane, and (d) acetonitrile.

Computational Method. The Gaussian 03 program[37] was used for the ab initio and DFT calculations. The 6-311G** basis set was used for all calculations unless otherwise noted. The torsional potentials were calculated by the HF, MP2,[38] and DFT (B3LYP)[39,40] methods using the HF level optimized geometries. The torsional angle was fixed, and other geometrical parameters were fully optimized in the torsional potential calculations. The excitation energies were calculated using the CIS,[41] CIS(D),[42] and time-dependent DFT (TD-DFT)[43] methods. The BHHLYP and B3LYP functionals were used for the DFT calculations.[39,40] The CIS and CIS(D) calculations were carried out using the HF and MP2 level optimized geometries, respectively. The TD-DFT calculations were carried out using the geometries optimized by the DFT calculations with the same functionals. The HOMOs and LUMOs shown in Figure 4 and Figures S4−S6 in Supporting Information were calculated at the HF/6-311G** level using the MP2/6-31G* level optimized geometries. The frozen-core approximation was applied for the MP2 calculations.

Results and Discussion

1. Absorption and Fluorescence Properties in Solution. ***1.1. Absorption Properties.*** Figures 1 and 2 show the absorption spectra of **2** and **3** in solution, respectively. Table 1 summarizes the absorption maxima (λ_a) in various kinds of solvents with different polarity. The data of **1** are shown in Figure S1 (Supporting Information) for comparison. Although the spectra

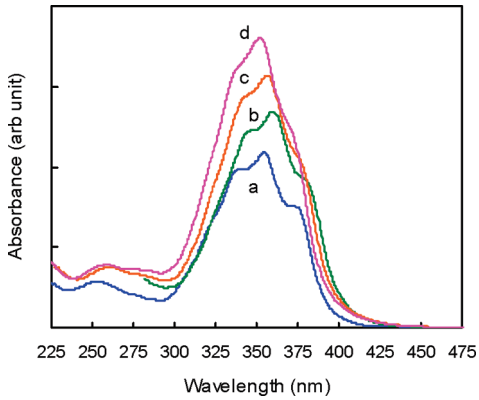

Figure 2. Absorption spectra of **3** in (a) methylcyclohexane, (b) toluene, (c) dichloromethane, and (d) acetonitrile.

of **4** have been reported previously by us[20] and others,[32,44] they are shown in Figure S2 (Supporting Information) and summarized in Table S1 (Supporting Information) for readers' convenience.

In the spectra of **2**, two broad bands were observed around 380 and 330 nm in all solvents studied. The relative intensity of the band at 380 nm to that at 330 nm significantly decreased with increasing solvent polarity, and the positions of λ_a moved slightly. The spectrum thus showed only a small dependence on the polarity of solvent. To understand the solvent-induced spectral shifts more quantitatively, the relationship between λ_a and the Onsager polarity functions, $f(n^2) = (n^2 - 1)/(2n^2 + 1)$ and $f(\epsilon_s) = (\epsilon_s - 1)/(2\epsilon_s + 1)$, where n is the refractive index and ϵ_s is the static dielectric constant, was investigated.[45−48] The plots of λ_a in wavenumber as a function of $f(n^2)$ exhibit a weak linear correlation (Figure S3(a) in Supporting Information). Although the correlation is rather poor, the slopes of the linear fits for the bands around λ_a = 380 and 330 nm are calculated to be −16030 and −4730 cm^{-1}, respectively. This suggests that the absorption around 380 nm is more strongly dependent on $f(n^2)$ than that around 330 nm. On the other hand, the plots of λ_a as a function of $f(\epsilon_s)$ show no significant correlation, even for the solvents having similar values of n (Figure S3(b) in Supporting Information).

In **3**, λ_a was observed at 373 nm (0−0) with its vibrational progressions at 355 nm (0−1) and 340 nm (0−2) in methylcyclohexane (MCH) solvent. Among them the 0−1 peak was the strongest in intensity. The energy spacings were 1243 and 1359 cm^{-1}, corresponding to the C═C and C—C stretches of conjugated trienes.[49,50] The solvent effects on the spectrum were small. The spectral shapes did not change greatly, although the spectrum was less structured in AN than in MCH. Even when the solvent changed from low polar MCH to highly polar AN, the peak positions shifted only slightly. Interestingly, however, the plot of λ_a in wavenumber as a function of $f(n^2)$ displays a reasonably good linear correlation with a slope of −11360 cm^{-1} (Figure S3(a) in Supporting Information). Whereas, if solvents of similar n values are considered, the plot of λ_a versus $f(\epsilon_s)$ shows a linear correlation with a slope of −490 cm^{-1} (Figure S3(b) in Supporting Information). From the results it may be possible that the solvent-induced shift of this absorption band is dominated mainly by dispersion interaction.[46,47] The positions of λ_a of **3** were very near to those of **1** in all solvents examined (Figure S1 in Supporting Information).

The spectrum of **4** in MCH showed λ_a at 395 nm (0−1) as the highest peak and some vibrational structures. The spacings of 1209 and 1393 cm^{-1} were similar to the values in **3**. As the solvent polarity increased, λ_a red-shifted from 395 nm in MCH to 422 nm in DMF. The spectrum became more structureless, probably due to the increased solute−solvent interactions. Here, the spectra in methanol and in AN were very similar, suggesting that the structureless features in polar solvents were not due to the intermolecular hydrogen bonds. The solvent effects on the spectrum in **4** were thus small but significantly larger than those in **2** and **3**. In contrast to the cases of **2** and **3**, however, the plot of λ_a in wavenumber as a function of $f(n^2)$ shows no correlation in **4** (Figure S3(a) in Supporting Information). On the other hand, for solvents with similar n, the plot of λ_a versus $f(\epsilon_s)$ shows the decrease in the energy of λ_a with the increase in $f(\epsilon_s)$ (Figure S3(b) in Supporting Information). Although the plot exhibits only a loose correlation, the slope of the linear fit is calculated to be −4260 cm^{-1}. The dependence of λ_a on $f(n^2)$ and $f(\epsilon_s)$ in **4** clearly differs from those in **2** and **3**.

1.2. Ground-State Geometries and Transition Assignments. *Ground-State Geometries.* The relative energies for the three kinds of conformational isomers (conformers) of **2** (A, B, and C in Chart S1 in Supporting Information) were calculated at the MP2/6-311G**//MP2/6-311G** level.[51] Conformer A is shown to be 2−3 kcal/mol more stable than B and C, suggesting that A is the major isomer and the populations of B and C are less than 3% at room temperature. The optimized geometrical parameters for A, whose structure is shown in Chart 1, are summarized in Table 2. The C1−C6−C7−C8 (Ar—CH═) and O1−N1−C1−C6 (Ar—NO_2) torsional angles are −150.0° and 37.6°, respectively (MP2/6-311G**), showing somewhat twisted conformation of the molecule. The O1 atom of the nitro group and the H7 atom of the triene are in close proximity in the optimized structure, which suggests the existence of attractive electrostatic interaction between O1 and H7. In this case it is very likely that there exists the weak intramolecular C−H···O hydrogen bond of the type described by Desiraju and Steiner.[53,54] The major geometrical parameters for the hydrogen bond are given in Table 3. The π-conjugation and the hydrogen bonding decrease the torsional angles, while the steric repulsion between O1 and H7 and between H5 and H8 atoms increases the angles. The somewhat twisted conformation of **2** is thus a result of the balance of these interactions.

We also calculated the relative energies for the three conformers for **3** (A, B, and C in Chart S2 (Supporting Information)) to find that A was slightly (0.3−0.6 kcal/mol) more stable than B and C. The small energy differences suggest that molecule **3** exists as a conformational mixture at room temperature in solution. Table 4 shows the results of optimization for conformer A, which is found in the X-ray determined crystal structure as described later. The results for molecule **4** are summarized in Table 5. As can be seen, the optimized structures of **3** and **4** are more planar than the structure of **2**. Here it should be noted, however, that the torsional angles of the Ar—CH═ single bonds in **3** (C6−C5−C7−C8) and **4** (C5−C4−C7−C8) given by the DFT calculations with BHHLYP and B3LYP functionals are significantly smaller than those calculated by the HF and MP2 methods. Similar discrepancies between the MP2 and B3LYP structures are reported for oligo(thiophene)s.[55−57]

Tables 2, 4, and 5 show the calculated values of bond length alternation (BLA). BLA refers to the difference between the averaged values of single (C—C) and double (C═C) bonds. It is one of the most important structural parameters that characterize the electronic and optical properties of one-dimensional conjugated compounds such as polyenes and polyynes, since it strongly affects the band gap of these molecules.[58,59] For each

TABLE 2: Major Geometrical Parameters for the X-ray and Optimized Structures of 2

	X-ray		calcd values[a]			
	molecule A[b]	molecule B[b]	HF	MP2	BHHLYP	B3LYP
			torsion angle (degree)			
C1–C6–C7–C8	–163.9(1)	–160.3(1)	–147.5	–150.0	–153.5	–158.6
O1–N1–C1–C6	22.8(2)	36.1(2)	28.0	37.6	24.8	25.5
			bond length (Å)			
C6—C7 (r_1)	1.469(2)	1.469(2)	1.480	1.465	1.463	1.463
C7═C8 (r_2)	1.344(2)	1.342(2)	1.327	1.358	1.335	1.352
C8—C9 (r_3)	1.437(2)	1.438(2)	1.459	1.442	1.440	1.438
C9═C9* (r_4)	1.351(3)	1.348(3)	1.330	1.362	1.338	1.355
BLA[c]	0.107	0.110	0.142	0.094	0.116	0.098

[a] The 6-311G** basis set was used. [b] Crystallographically independent two molecules. Each molecule has a center of symmetry. [c] Bond length alternation; BLA = $(r_1 + r_3)/2 - (2r_2 + r_4)/3$. For atom numbering, see Chart 1.

TABLE 3: Intramolecular Hydrogen Bond Geometry for 2

	X-ray		
	molecule A[a]	molecule B[a]	calcd[b]
d(O1···H7)[c] (Å)	2.269	2.391	2.432
d(O1···C7)[c] (Å)	2.768(2)	2.814(2)	2.781
C7H7O1 (deg)	111.9	106.6	96.9

[a] Crystallographically independent two molecules. [b] At the MP2/6-311G** level. [c] *d*: distance. For atom numbering, see Chart 1.

TABLE 4: Major Geometrical Parameters for the X-ray and Optimized Structures of 3

	X-ray		calcd[a]			
	molecule A[b]	molecule B[b]	HF	MP2	BHHLYP	B3LYP
			torsion angle (degree)			
C6—C5—C7—C8	−4.6(3)	−0.6(3)	11.0	22.4	0.1	0.0
O2—N1—C1—C6	−5.8(2)	−1.9(2)	−0.7	−11.7	0.0	0.1
			bond length (Å)			
C5—C7 (r_1)	1.470(2)	1.466(2)	1.475	1.463	1.459	1.460
C7═C8 (r_2)	1.338(2)	1.335(3)	1.329	1.359	1.336	1.352
C8—C9 (r_3)	1.447(2)	1.435(2)	1.458	1.441	1.439	1.437
C9═C9* (r_4)	1.345(3)	1.338(4)	1.331	1.363	1.339	1.356
BLA[c]	0.119	0.115	0.137	0.092	0.112	0.095

[a] The 6-311G** basis set was used. [b] Crystallographically independent two molecules. Each molecule has a center of symmetry. [c] Bond length alternation; BLA = $(r_1 + r_3)/2 - (2r_2 + r_4)/3$. For atom numbering, see Chart 1.

TABLE 5: Major Geometrical Parameters for the X-ray and Optimized Structures of 4

		calcd[b]			
	X-ray[a]	HF	MP2	BHHLYP	B3LYP
		torsion angle (degree)			
C5—C4—C7—C8	18.0(2)	14.8	23.1	0.0	0.0
C11—C12—C13—C14	−0.7(2)				
O2—N1—C1—C6	−1.4(2)	0.0	8.1	0.1	−0.1
O3—N2—C16—C15	2.7(2)				
		bond length (Å)			
C4—C7 (r_1)	1.459(2)	1.474	1.462	1.457	1.457
C7═C8 (r_2)	1.340(2)	1.329	1.360	1.337	1.353
C8—C9 (r_3)	1.437(2)	1.457	1.441	1.438	1.435
C9═C10 (r_4)	1.342(2)	1.331	1.363	1.340	1.357
C10—C11 (r_5)	1.437(2)				
C11═C12 (r_6)	1.341(2)				
C12—C13 (r_7)	1.457(2)				
BLA[c]	0.107	0.136	0.091	0.110	0.092

[a] Reference 72. [b] The 6-311G** basis set was used. [c] Bond length alternation. For the X-ray structure, BLA = $(r_1 + r_3 + r_5 + r_7)/4 - (r_2 + r_4 + r_6)/3$. For the optimized structures, BLA = $(r_1 + r_3)/2 - (2r_2 + r_4)/3$. For atom numbering, see Chart 1.

molecule, BLA from HF is larger than, and those from MP2 and B3LYP are smaller than those determined by X-ray analyses. BLA from BHHLYP is in fairly good agreement with the experimental values, as in the cases of a donor−acceptor diphenylpolyene[60] and polyacetylene oligomers.[61]

Torsional Potentials. Figure 3 shows the torsional potentials for **2** that were calculated by rotating the Ar—CH═ or Ar—NO_2 torsional angle of the most stable conformer A at the MP2/6-311G**//HF/6-311G** level. The barrier heights for the internal rotation around these bonds are approximately 4.5 kcal/mol (Ar—CH═) and 2.0 kcal/mol (Ar—NO_2). The low barrier heights suggest that the rotation around these bonds occurs nearly freely at room temperature in solution. In the figure, we see that the Ar—CH═ angles for most of the molecules are in the range of 115−240° and the Ar—NO_2 angles are in the range of 0−70 or 115−180°. The potentials are shallow in a wide range of torsional angles around the minima, suggesting that these bonds have various torsional angles at room temperature in solution (i.e., the presence of various kinds of conformers in equilibrium).

As reported earlier, the barrier height for the internal rotation in styrene is calculated to be about 2.5 kcal/mol (MP4(SDQ)/6-31G//HF/6-31G*)[62] and that in nitrobenzene is about 4.8 kcal/mol (MP2/6-311G**//HF/6-31G*).[63] These are close to experimental values.[62,63] The energy barrier for the Ar—CH═ bond in **2** is higher than that in styrene. This is probably due to the large steric repulsion between O1 and H8 in **2**, which is absent in styrene. On the other hand, the barrier height for the Ar—NO_2 rotation in **2** is lower than that in nitrobenzene. In nitrobenzene, the planar structure is the most stable, as the steric repulsion between the O atom of the nitro group and the aromatic H at the ortho position relative to the nitro group is small.[64] While in **2**, the planar structure is enhanced in energy and no longer the energy minimum because of the steric repulsion between O1 and H7. In this case, the somewhat twisted structure with the Ar—NO_2 torsional angle of around 150° becomes the most stable. This results in the low barrier height for the rotation of Ar—NO_2 bond in **2** relative to that in nitrobenzene. Thus the calculated barrier heights for the rotation of Ar—CH═ and Ar—NO_2 bonds in **2** are consistent with those reported for styrene and nitrobenzene, respectively.

Figure 3 also shows the torsional potentials for the Ar—CH═ and Ar—NO_2 bonds calculated by the HF and B3LYP methods using the HF level geometries for comparison. The barrier heights for the rotation of Ar—CH═ bond obtained by the HF and B3LYP methods are 4.8 and 5.9 kcal/mol, respectively. The barrier heights for the Ar—NO_2 bond by the two methods are 2.7 kcal/mol (HF) and 2.9 kcal/mol (B3LYP). These values are not greatly different from those obtained by the MP2 method. Also the potential minima are found in a similar region of

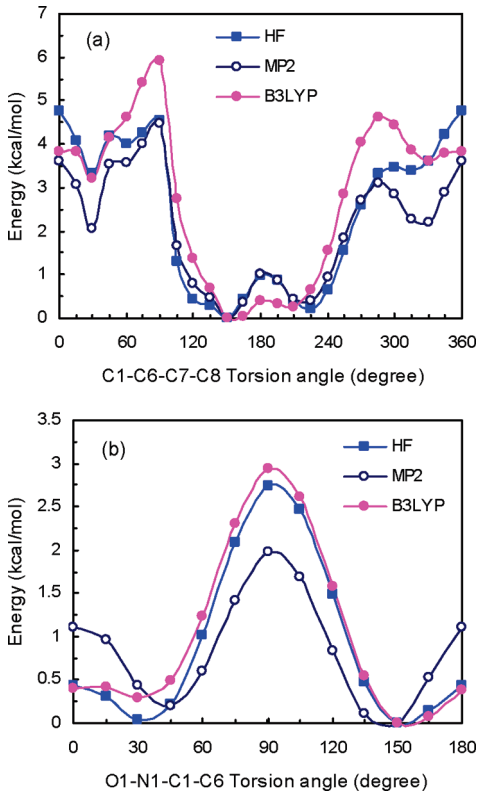

Figure 3. Torsional potentials for (a) C1−C6−C7−C8 and (b) O1−N1−C1−C6 bonds of **2** calculated by the HF, MP2, and B3LYP methods using the HF level optimized geometries. The 6-311G** basis set was used. For atom numbering, see Chart 1. The solid lines are only guides for the eyes.

torsional angles for the Ar−CH= and Ar−NO_2 rotation, although the details are somewhat different.

The barrier heights for the internal rotation around Ar−CH= and Ar−NO_2 bonds in **3** and **4** will be close to the values in styrene and nitrobenzene molecules, respectively. Considering the low barrier heights calculated for styrene and nitrobenzene mentioned above, we can expect that the rotation around Ar−CH= and Ar−NO_2 bonds in **3** and **4** is almost free in solution.

Vertical Excitation Energies. To understand the electronic transitions for the absorption bands of **2**−**4**, vertical excitation energies were calculated using the optimized structures for the most stable conformers. The results are summarized in Tables S2−S4 in Supporting Information.

For all three molecules, the CIS method gave considerably higher excitation energies than the experimental values determined from the absorption spectra. The overestimation of the excitation energies by CIS has been reported for other short polyenes.[65,66] The CIS(D) method gave the energies lower by approximately 30 nm than those by CIS, approaching the experimental values considerably. The improvement is probably due to the fact that CIS(D) considers the double excitation, which is important for polyene molecules[65,66] but absent in CIS.[42,67]

In contrast, the TD-B3LYP calculations yielded the excitation energies lower than those from the experiments. Typically, TD-DFT fails to describe precisely the excited states with substantial charge transfer (CT) or double excitation character,[60,67] especially in extended π-electron conjugation systems.[66] In our case, the BHHLYP functional gave the excitation energies higher than those from B3LYP. Similar results are reported for a donor−acceptor diphenylpolyene.[60] The values from TD-BHHLYP are the nearest to the experiments among the results of the present calculations. The calculated excitation energy of **1** is very similar to the value of **3**, in agreement with the experiments.

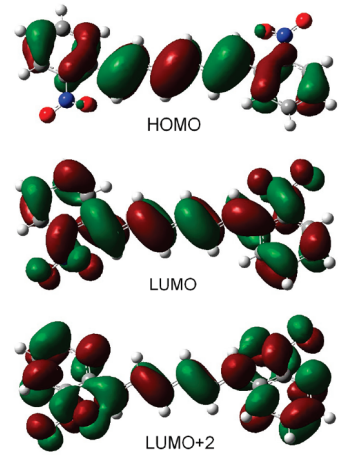

Figure 4. HOMO, LUMO, and LUMO+2 of **2**.

Assignments of Transition. The calculations show that the two absorption bands around 380 and 330 nm observed in the spectrum of **2** are mainly due to the electronic transition from HOMO to LUMO and that from HOMO to LUMO+2, respectively (Table S2 in Supporting Information). Figure 4 shows the HOMO, LUMO, and LUMO+2 in the optimized structure. These orbitals are delocalized over the whole of the molecule, indicating the effective π-delocalization between the nitro group and DPH moiety. Clearly, significant CT from the aromatic DPH to the nitro group occurs associated with the HOMO−LUMO and HOMO−LUMO+2 transitions. In LUMO+2, the π-orbitals of O1 and C7 atoms are in close proximity to each other. This indicates that the cooperative twists along the Ar−NO_2 and Ar−CH= single bonds are important for the HOMO−LUMO+2 transition. Further, this explains the fact that no corresponding band was observed in the spectra of **3** and **4**. For *o*,*o*′-dinitro-substituted 1,4-diphenyl-1,3-butadiene (DPB), two absorptions are similarly observed at 340 and 278 nm in its solution spectrum.[30]

The absorption band centered at 355 nm in **3** is mainly due to the HOMO−LUMO transition, although contribution from HOMO−LUMO+2 is also significant in the TD-B3LYP calculation (Table S3 in Supporting Information). Also in **3**, the HOMO−LUMO transition has CT character from DPH to the nitro group. On the other hand, the absorption at 354 nm in **1** is assigned to the HOMO−LUMO transition with $\pi-\pi^*$ character. Although the spectral features of **1** and **3** were very similar, the nature of the transition was thus entirely different.

The absorption at 395 nm in **4** is assigned to the HOMO−LUMO transition (Table S4 in Supporting Information). The HOMO and LUMO indicate the effective π-delocalization between the nitro group and DPH. The absorption is clearly due to the CT transition from DPH to the nitro group. The HOMOs and LUMOs of **1**, **3**, and **4** are displayed in Figures S4−S6 of the Supporting Information.

1.3. Fluorescence Properties. Molecule **2** was nonfluorescent in all solvents studied. The optimized structure suggests the existence of the C−H···O intramolecular hydrogen bonds in the ground state. In this case, the excited-state intramolecular proton transfer (ESIPT) along the hydrogen bonds will occur within a very short time domain,[68,69] although the C−H···O hydrogen bonds are considered to be rather weak compared to

the typical ones like N−H···O and O−H···O. The resulting ionic species from ESIPT in the singlet excited state will rapidly deactivate nonradiatively by IC to the ground state. In the efficient IC from such an ionic species, out-of-plane torsional motions associated with the hydrogen bonds are shown theoretically to be important.[69] Also, IC in **2** can involve the twisting motion around the Ar−NO_2 bond, as suggested for nitroperylene in aprotic solvents like AN.[24]

Molecule **3** exhibited fluorescence only in medium polar solvents such as 1,4-dioxane and THF. Table 1 summarizes the fluorescence data, and Figure 5 shows the absorption and emission spectra in solution. The fluorescence spectra showed no dependence on the excitation wavelength. The fluorescence excitation spectra were essentially the same as the absorption spectra and showed no dependence on the emission wavelength. As the solvent polarity increased from carbon tetrachloride to THF, λ_f red-shifted by 92 nm from 482 to 574 nm. The observation is in sharp contrast to the fact that only a small solvent dependence was observed in λ_a. As a result of this, the Stokes shift (ΔE_{ss}) increased from 7186 cm^{-1} in carbon tetrachloride to 10589 cm^{-1} in THF. Accordingly, the overlap between the absorption and emission spectra was very small or almost none. The position of λ_f moved to longer wavelengths with increasing solvent polarity, suggesting that the emissive state was more stabilized in more polar solvents. The emission of **3** will therefore originate from an intramolecular charge transfer state (ICT*), formed from an initially photoproduced, locally excited state (LE*). Unlike the weakly structured absorption spectra, the emission spectra were all broad and structureless, although the spectrum in carbon tetrachloride was rather noisy. These spectral features are also characteristic of the ICT* emission.

Fluorescence lifetime (τ_s) and ϕ_f data are shown in Table 1. The fluorescence decay curves were able to be analyzed by monoexponential function to give τ_s of 1−2 ns. The value of ϕ_f increased with an increase in solvent polarity to reach the maximum in medium polar solvents and fell again. The low ϕ_f can be attributed to small radiative rate constants ($k_f = \phi_f/\tau_s$) on the order of 10^5-10^6 s^{-1}, consistent with the weakly forbidden nature of the ICT* transition.[70]

Despite the spectral similarity in the absorption of **1** and **3**, the highly solvent-dependent fluorescence behavior of **3** differed entirely from that of **1** (Figure S1 in Supporting Information). It is quite reasonable that the nitro groups in **3**, which are absent in **1**, play an essential role in the formation of ICT*.

The fluorescence spectra of **4** are shown in Figure S7 (Supporting Information) and summarized in Table S1 (Supporting Information). Although the emission properties of **4** in solution have been reported previously,[20] here we describe the results briefly to compare them with those of **3**. The fluorescence spectrum was structured with λ_f of 460 nm in low polar MCH, whereas in polar AN the spectrum became broad and structureless and λ_f dramatically red shifted to 580 nm. The fluorescence origin of **4** was determined to be LE* in low polar solvents such as MCH and carbon tetrachloride, LE* and ICT* (dual fluorescence) in medium polar solvents such as THF and chloroform, and ICT* in highly polar solvents such as DMF and AN. These assignments were based on the steady-state and picosecond time-resolved fluorescence data in various kinds of solvents with different polarity. It is worth noting that the position of λ_f in AN further red shifted to 654 nm in methanol, and ϕ_f in this solvent was much lower than the value in AN (Table S1 in Supporting Information). The observation in methanol probably results from the intermolecular hydrogen bonds between solute and solvent.

For **3**, the plot of λ_f in wavenumber as a function of $f(\epsilon_s) - f(n^2)$ exhibits no linear correlation. The plot for **4** shows the decrease in the energy of λ_f with the increase in $f(\epsilon_s) - f(n^2)$ (Figure S8 in Supporting Information). However, it exhibits only a poor correlation, probably due to the complex nature of dual fluorescence.

The strong solvent dependence of ϕ_f was similar for **3** and **4**. The low ϕ_f in polar solvents can be attributed to the efficient IC due to the lowered energies of ICT* ("the energy-gap low").[70] Whereas, in low polar solvents, ISC rates should probably be considered. In the case of **4**, the quantum yield of ISC increased from <0.01 in AN to 0.89 in MCH.[20]

2. Absorption and Fluorescence Properties in the Solid State. Figure 6 shows the absorption, fluorescence, and fluorescence excitation spectra of crystals **2**−**4**. The absorption and fluorescence data are summarized in Table 6.

2.1. Absorption Properties. In the absorption spectrum of **2**, λ_a was observed at 505 nm. Unlike that, two bands of different electronic origins were observed in solution, only one broad band was seen in the solid state.

In the spectrum of **3**, we observed a main peak at 432 nm and two weak peaks at 398 and 372 nm. The energy spacings for them were 1756 and 1978 cm^{-1}, somewhat larger than the typical values for the C═C and C−C stretches of conjugated trienes.[49,50] It is unclear whether these weak peaks are the vibrational progressions of the main peak or not.

In **4**, a peak at 508 nm and its vibrational progressions at 474 and 441 nm were observed. The spacings of 1412 and 1579 cm^{-1} were similar to the values in solution.

For all three molecules, λ_a in the solid state red shifted compared to those in solution. From λ_a of the longer wavelength band of **2** and those of the 0−1 peaks of **3** and **4** in MCH solution shown in Table 1 and Table S1 (Supporting Information), and λ_a in the solid state shown in Table 6, the red shifts for **2**, **3**, and **4** were calculated to be 6865, 5021, and 5631 cm^{-1}, respectively. The shift for **2** was clearly larger than the shifts for **3** and **4**, thus leading to similar λ_a for **2** and **4** in the solid state. Note that λ_a of **4** in solution was located at a longer wavelength than that of **2**.

2.2. Fluorescence Properties. The solid-state fluorescence spectra were all broad and structureless. In contrast to the fact that no emission from **2** was observed in solution, its fluorescence spectrum was measurable in the solid state. Although ΔE_{ss} of **3** was somewhat larger than those of **2** and **4** (Table 6), the overlap of the absorption (or the fluorescence excitation) and fluorescence spectra was considerably large for each molecule (Figure 6).

As the origin of the solid-state fluorescence, monomeric (LE* and ICT*) and excimeric (or excimer-like) species, and molecular aggregates having the ground-state energy minima and thus their own absorption bands, would be possible. In the present case, no dependence of fluorescence spectrum on the excitation wavelength was observed, the fluorescence excitation spectra were fundamentally the same as the absorption spectra, and the excitation spectra showed no dependence on the emission wavelength. These strongly suggest that the fluorescence of **2**−**4** derives not from the ground-state molecular aggregates but from the monomeric or excimeric species. Further, by considering the relatively large absorption−fluorescence spectral overlaps, we can conclude that the fluorescence from crystals **2**−**4** originates from the monomeric LE* states.

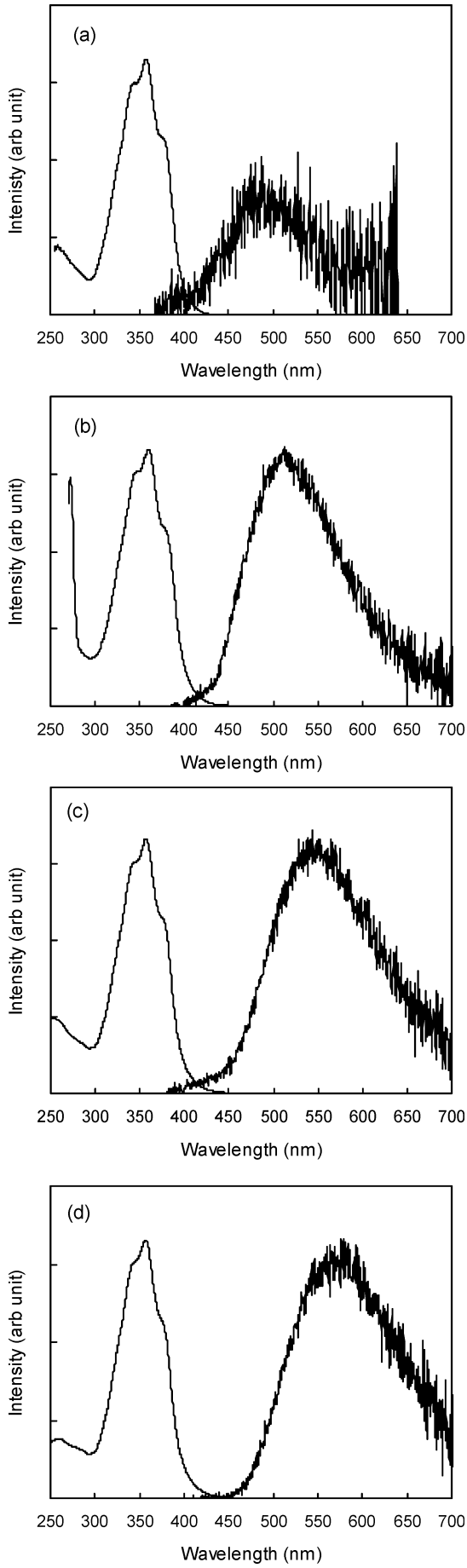

Figure 5. Absorption and fluorescence spectra of **3** in (a) carbon tetrachloride, (b) toluene, (c) 1,4-dioxane, and (d) tetrahydrofuran.

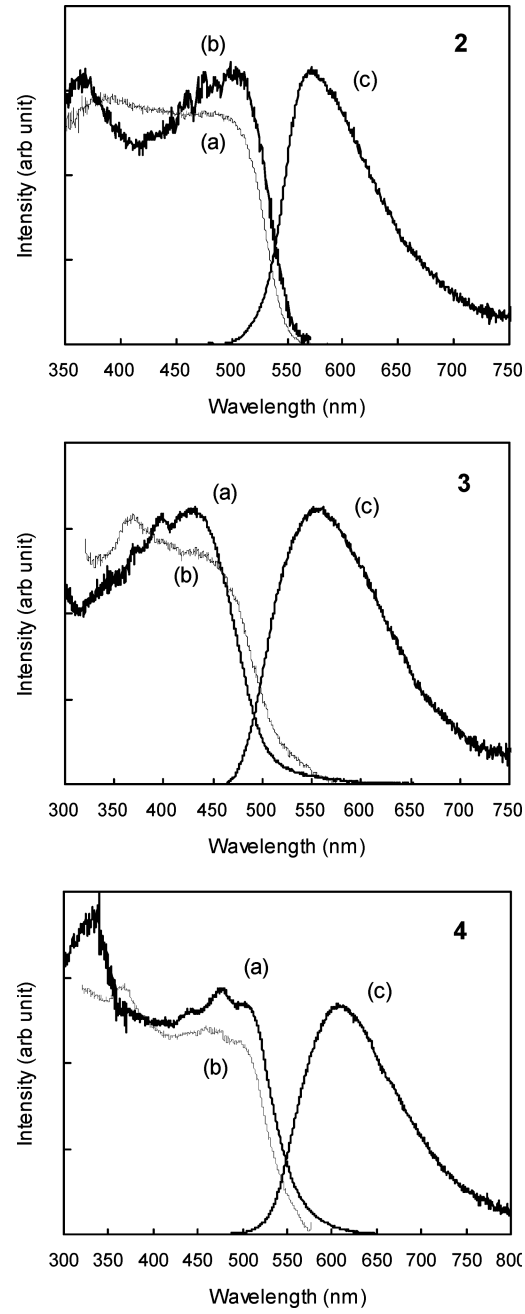

Figure 6. (a) Absorption, (b) fluorescence excitation, and (c) fluorescence spectra of crystals **2**−**4**.

TABLE 6: Absorption and Fluorescence Data for Crystals 2−4

compound	λ_a (nm)	λ_{exc}[a] (nm)	λ_f (nm)	ΔE_{ss}[b] (cm^{-1})	ϕ_f
2	505	503	570	2258	0.0046
3	432	439	559	5259	0.0079
4	508	504	613	3372	0.0068

[a] The maximum wavelength in the fluorescence excitation spectrum. [b] Calculated from λ_a and λ_f.

The solid-state ϕ_f values of **2**−**4** were small (Table 6), and their fluorescence decay curves were similar. Although the perfect analysis of the decay curve was impossible due to small ϕ_f and intrinsic inhomogeneity of solid samples, τ_s for crystals **2**−**4** were roughly estimated by single-exponential fitting to be 0.9−1 ns. Values τ_s of 1−2 ns are typical for the single-molecule fluorescence of small organic dyes in the solid state.[18,71]

TABLE 7: Crystal Data of 2−4

	2	3	4[a]
formula	$C_{18}H_{14}N_2O_4$	$C_{18}H_{14}N_2O_4$	$C_{18}H_{14}N_2O_4$
formula weight	322.31	322.31	322.31
crystal color, habit	yellow, needle	yellow, needle	yellow, needle
crystal size (mm)	0.45 × 0.07 × 0.05	0.30 × 0.10 × 0.07	0.30 × 0.25 × 0.02
crystal system	monoclinic	triclinic	monoclinic
space group	$P2_1/n$	P-1	$P2_1/c$
a (Å)	19.341(2)	6.306(1)	3.8710(4)
b (Å)	3.8902(4)	10.849(2)	21.440(2)
c (Å)	20.212(2)	12.374(2)	18.709(2)
α (deg)	90	107.847(3)	90
β (deg)	90.594(2)	98.976(3)	95.555(2)
γ (deg)	90	103.827(3)	90
V (Å^3)	1520.7(3)	758.0(2)	1545.4(3)
Z	4	2	4
D_{calc} (g/cm^3)	1.408	1.412	1.385
T (°C)	−90	−90	−90
mp (°C)	231	236	241
R_1 ($I > 2\sigma(I)$)	0.0444	0.0482	0.0400

[a] Reference 72.

3. Crystal Structures. Table 7 shows the single-crystal data of **2**−**4** obtained by X-ray structure analyses.

3.1. Molecular Structures. The major geometrical parameters for the structures of **2**−**4** are depicted in Tables 2, 4 and 5.

In the crystal structure of **2**, torsional angles of Ar−CH= and Ar−NO_2 are −160 to −165° and 20−35°, respectively. This indicates that the molecules are nearly but not completely planar even in the solid state. Molecules **3** and **4** have more planar conformations in crystals.

As in the optimized structure, the C−H···O intramolecular hydrogen bonds will exist in crystal **2**. In Table 3, we compare the geometrical parameters for the hydrogen bond in the MP2 optimized and X-ray determined molecular structures. Although the angle of C−H···O is somewhat larger in the X-ray structures, the distances of d(O1···H7) and d(O1···C7) are not largely different for these structures.

3.2. Molecular Arrangements. The crystal packing diagrams for **2**−**4** are shown in Figure S9 in Supporting Information.

In the crystal structure of **2**, there exist two crystallographically independent molecules, A and B. Each molecule has a center of symmetry. Molecules A and B are linked to each other by the intermolecular C−H···O hydrogen bonds between the O atoms of the nitro groups and the H atoms of the aromatic rings or the trienes to form sheetlike structures. These sheets are piled up along the b axis with the interplane distance of 3.49 Å for the stacking of two molecules of A and 3.55 Å for those of B. For the nearest molecules of A and B in the sheet, the dihedral angles for the least-squares planes of DPH (18 carbons) are 18.29° between A and B and 45.49° between A and B′ (molecule B′ is related a screw axis with B; see Figure S9 (Supporting Information)).

Also in **3**, two crystallographically independent molecules, A and B, are contained in the unit cell. Molecules A and B are each linked through the intermolecular C−H···O hydrogen bonds between the O atoms of the nitro group and the H atoms of the aromatic ring at the ortho position relative to the nitro group. A pair of this type of hydrogen bonds makes a hexagonal pattern between the nearest molecules along the long molecular axis to form one-dimensional tapes of ···A···A···A··· and ···B···B···B···. These tapes are arranged in a herringbone fashion. The dihedral angle made by the DPH planes for the nearest molecules of A and B is 83.49°.

The structure of **4** was reported previously.[72] As in **2**, the molecules in this structure are linked via intermolecular C−H···O hydrogen bonds to make sheets. In the sheets, the dihedral angle between the DPH planes of the nearest molecules is 8.28°. The molecular coplanarity in **4** is thus higher than that in **2**. The sheets stack further along the a axis with an interplane distance of 3.47 Å by N···O dipole−dipole and $\pi-\pi$ stacking interactions.

Thus, although linked by similar types of intermolecular hydrogen bonds, the molecules are arranged very differently in each crystal, depending on the position of the nitro substituent on the benzene ring.

4. Effects of Intramolecular Planarization and Intermolecular Interactions. ***4.1. Absorption Properties.*** For all molecules, λ_a in the solid state red shifted from those in solution. The spectral red shifts should mainly be attributed to the planarization of molecules and the intermolecular interactions in crystals.

The red shifts were 5021 cm^{-1} for **3** and 5631 cm^{-1} for **4**. In **3**, the molecules experienced almost complete planarization from solution to the solid state, as shown by the X-ray analysis. This results in more effective π-delocalization, leading to a considerable red shift of λ_a in the solid state. The degree of molecular planarization in **4** was similar to (or somewhat smaller than) that in **3**, and thus the spectral shifts due to planarization would not be very different for **3** and **4**, although the red shift due to planarization around Ar−NO_2 may be somewhat different for each. Therefore, the small difference of approximately 600 cm^{-1} between the total red shifts of **3** and **4** suggests that the shifts due to intermolecular interactions are also similar for **3** and **4**. The intermolecular interactions in crystal **3** are expected to be small, considering its herringbone structure. Consequently, the effects of intermolecular interactions on the spectrum should be similarly small in crystal **4** having π-stacked structure.

The spectral shift for **2** (6865 cm^{-1}) was clearly larger than that for **4**. On comparison of the molecular arrangements in crystals **2** and **4**, it is unlikely that the intermolecular interactions in **2** are much larger than those in **4** to induce a large spectral difference between them. Thus, we can safely say that the spectral shift due to the interactions in **2** is small as in **4**. Accordingly, the larger red shift in **2** should be attributed to the larger shift due to molecular planarization in the solid state. This is somewhat unexpected, because molecule **2**, unlike **4**, is nearly planar but still distorted to some extent even in the solid state.

The torsional potentials of **2** for the most stable conformer A are shallow in a wide range of angles around the minima (Figure 3). The flatness of the potential in the ground state suggests that the observed absorption spectrum in solution is a superposition of spectra for the various kinds of conformers equilibrated in solution. For oligo(*p*-phenyleneethynylene)s, the potential for the twisting of phenyl group in the excited state is shown to be similar in shape to that of the ground state, but more strongly dependent on the torsional angle than in the ground state.[73,74] The results are used to interpret their conformation-dependent spectroscopic phenomena observed in ensemble and single molecule spectroscopy. If we assume that this is also the case for our present molecules, then the larger red shift in **2** than in **4** may be explained by the larger angle-dependence of potential for **2** in the excited state.

Thus, the red shifts in the absorption spectra for **2**−**4** are mainly attributed to the intramolecular planarization in the solid state. The effects of intermolecular interactions on the spectra appear to be relatively small in these crystals.

4.2. Fluorescence Properties. Although **2** was completely nonfluorescent in solution, the molecule exhibited measurable fluorescence in the solid state. This can be attributed to the

restricted torsional motions in the solid state. As described above, the intramolecular motions can possibly increase the IC efficiency of **2** in solution. The enhancement of the solid-state fluorescence intensity due to molecular planarization in the excited state and the suppression of nonradiative torsional deactivation has been considered for distyrylbenzenes.[12]

The fluorescence from crystals **2**−**4** was of all monomeric origin, consistent with the relatively small effects of intermolecular interactions on the absorption spectra. The LE* states of **3** and **4** responsible for the solid-state emission are expected to be almost completely planar, as those observed in the crystal structures. Therefore, no observation of ICT* fluorescence in the solid state strongly suggests that the ICT* states of **3** and **4** responsible for the red-shifted emission in solution have twisted geometries (TICT).[75]

p-(Dimethylamino)benzonitrile (*p*-DMABN), one of the most well-known TICT molecules in solution, showed a single emission band originating from LE* in the crystalline state.[76] The results show that ICT does not occur in the crystalline *p*-DMABN, similar to our observations for **3** and **4**. We should note here, however, that the ICT* fluorescence of DMABN in solution was only observed for its *p*-derivative, and the ICT* emission from *m*-derivative has not been reported so far.[77]

In contrast to the case of **4**, we previously observed that the fluorescence behavior of *p*,*p*′-dicyano-substituted DPH was essentially independent of the solvent polarity.[20] Although the EW strength of the cyano group is significantly weaker than that of the nitro group, the difference in the fluorescence behavior between them appears to be too large to be understood only by the difference in the EW strength. To explain the results, we assumed a distorted geometry for ICT* of **4**. The twisting of Ar−NO_2 bond should lead to ICT* with strong CT character, resulting from electronic decoupling due to nearly perpendicular geometry of the π-planes of DPH and the nitro group, while twisting of the Ar−CN bond does not lead to complete decoupling between DPH and the cyano group because of the intrinsic nature of the C≡N triple bond. The evidence supporting this assumption has been provided by the present study.

p-(*n*-Alkoxy)-*p*′-nitro-substituted DPHs also exhibited LE* fluorescence of monomeric origin in the crystalline state.[18] Absence of ICT* emission in the solid state shows the red-shifted fluorescence in polar solvents to be originated from TICT*. The involvement of TICT was also suggested in the fluorescence behavior of nitro-cyano-substituted DPBs in solution.[78] Thus, TICT* fluorescence has been observed for several kinds of nitro-substituted diphenylpolyenes in solution and may be common in this class of compounds.

The effects of the intramolecular planarization on the fluorescence spectroscopic properties of **2**−**4** are considerably large, while those of the intermolecular interactions appear to be relatively small in these crystals. The results are in contrast to our previous observations for alkoxy-nitro-substituted[18] and fluorinated[19] DPHs, in which the intermolecular interactions in crystals greatly affected the solid-state spectroscopic properties. This suggests that, at least for one-dimensional conjugated molecules like DPH, the magnitude of the intermolecular interactions in crystals is highly sensitive to the relative positions of the π-orbitals of the linear conjugated chains of the interacting molecules. Depending on the molecular arrangements in crystals, the interactions can be strong enough to induce emission from excimeric or aggregated species as observed in some cases of fluorinated DPHs,[19] whereas, they can be rather weak only to have limited effects on the spectra as in the present molecules.

Conclusions

The absorption spectra of **2**−**4** in solution exhibited only a small dependence on the solvent polarity; however, λ_a were weakly correlated with the Onsager polarity functions. For these molecules, theoretical calculations suggest that the internal rotation around Ar−CH═ and Ar−NO_2 single bonds occurs almost freely, and various kinds of conformers are present at room temperature in solution. The calculated barrier heights for the rotation of Ar−CH═ and Ar−NO_2 bonds in **2** are consistent with those reported for styrene and nitrobenzene, respectively. The solid-state absorption spectra of **2**−**4** were red-shifted compared to those in solution. In the solid state, the torsional motions were restricted and molecules were frozen in nearly or almost completely planar conformations, as determined by the X-ray analyses. We can therefore expect considerable planarization of molecules in the solid state, which is mainly responsible for the spectral red shifts in the absorption. The molecular arrangement in each crystal was significantly different; however, the effects of intermolecular interactions on the absorption spectra appeared to be relatively small. Consistently, the origin of the solid-state fluorescence was all monomeric.

Although **2** was nonemissive in all solvents studied, the molecule exhibited measurable fluorescence in the solid state. The efficient NRD in solution would be due to very rapid IC from the proton-transferred ionic state produced by ESIPT along the CH···O hydrogen bonds. In the efficient IC, out-of-plane torsional motions possibly play an important role. The measurable fluorescence emission from crystal **2** can therefore be attributed to the restricted torsional motions in the solid excited state. The fluorescence of **3** in solution originated from ICT*, and that of **4** from LE*and/or ICT* depending on the solvent polarity. In contrast, they showed LE* fluorescence in the solid state. No observation of ICT* emission in crystals strongly suggests the twisted geometries for ICT* of **3** and **4** in solution. Thus, **3** and **4** provide new examples for TICT molecules.

Acknowledgment. We thank Dr. Y. Kawanishi (AIST) for the use of the fluorescence spectrometer, and Dr. K. Ohta (AIST) for valuable comments on the calculated results of vertical excitation energies and transition assignments. We also acknowledge Ms. S. Shibasaki (AIST) for the elemental analyses of **2**−**4**.

Supporting Information Available: Crystallographic data of **2** and **3** in CIF format; crystal and structure refinement data of **2**−**4**; chemical structures of conformational isomers of **2** and **3**; absorption and fluorescence spectra of **1** and **4** in solution; plots of λ_a and λ_f of **2**−**4** in solution versus the Onsager polarity functions; HOMOs and LUMOs of **1**, **3**, and **4**; crystal packing diagrams of **2**−**4**; vertical excitation energies of **2**−**4**; and full author list for ref 37. This material is available free of charge via the Internet at http://pubs.acs.org.

References and Notes

(1) Zollinger, H. *Color Chemistry, Syntheses, Properties and Applications of Organic Dyes and Pigments*, 3rd ed.; Wiley-VCH: Weinheim, Germany, 2003.
(2) Hung, L. S.; Chen, C. H. *Mater. Sci. Eng., R* **2002**, *39*, 143.
(3) Kulkarni, A. P.; Tonzola, C. J.; Babel, A.; Jenekhe, S. A. *Chem. Mater.* **2004**, *16*, 4556.
(4) Kelley, T. W.; Baude, P. F.; Gerlach, C.; Ender, D. E.; Muyres, D.; Haase, M. A.; Vogel, D. E.; Theiss, S. D. *Chem. Mater.* **2004**, *16*, 4413.
(5) Veinot, J. G. C.; Marks, T. J. *Acc. Chem. Res.* **2005**, *38*, 632.
(6) Burn, P. L.; Lo, S.-C.; Samuel, I. D. W. *Adv. Mater.* **2007**, *19*, 1675.
(7) Hide, F.; Díaz-García, M. A.; Schwartz, B. J.; Andersson, M. R.; Pei, Q.; Heeger, A. J. *Science* **1996**, *273*, 1833.

(8) Tessler, N.; Denton, G. J.; Friend, R. H. *Nature* **1996**, *382*, 695.
(9) Pei, Q.; Yu, G.; Zhang, C.; Yang, Y.; Heeger, A. J. *Science* **1995**, *269*, 1086.
(10) Abyan, M.; de Caro, D.; Fery-Forgues, S. *Langmuir* **2009**, *25*, 1651.
(11) Oelkrug, D.; Tompert, A.; Gierschner, J.; Egelhaaf, H.-J.; Hanack, M.; Hohloch, M.; Steinhuber, E. *J. Phys. Chem. B* **1998**, *102*, 1902.
(12) An, B.-K.; Kwon, S.-K.; Jung, S.-D.; Park, S. Y. *J. Am. Chem. Soc.* **2002**, *124*, 14410.
(13) Mizobe, Y.; Tohnai, N.; Miyata, M.; Hasegawa, Y. *Chem. Commun.* **2005**, 1839.
(14) Mizobe, Y.; Hinoue, T.; Yamamoto, A.; Hisaki, I.; Miyata, M.; Hasegawa, Y.; Tohnai, N. *Chem.—Eur. J.* **2009**, *15*, 8175.
(15) Turek, A. M.; Krishnamoorthy, G.; Sears, D. F., Jr.; Garcia, I.; Dmitrenko, O.; Saltiel, J. *J. Phys. Chem. A* **2005**, *109*, 293.
(16) Itoh, T. *J. Chem. Phys.* **2005**, *123*, 064302.
(17) Sonoda, Y.; Kawanishi, Y.; Ikeda, T.; Goto, M.; Hayashi, S.; Yoshida, Y.; Tanigaki, N.; Yase, K. *J. Phys. Chem. B* **2003**, *107*, 3376.
(18) Sonoda, Y.; Goto, M.; Tsuzuki, S.; Tamaoki., N. *J. Phys. Chem. A* **2006**, *110*, 13379.
(19) Sonoda, Y.; Goto, M.; Tsuzuki, S.; Tamaoki., N. *J. Phys. Chem. A* **2007**, *111*, 13441.
(20) Sonoda, Y.; Kwok, W. M.; Petrasek, Z.; Ostler, R.; Matousek, P.; Towrie, M.; Parker, A. W.; Phillips, D. *J. Chem. Soc., Perkin Trans. 2* **2001**, 308.
(21) Mesaros, M.; Bonesi, S. M.; Ponce, M. A.; Erra-Balsells, R.; Bilmes, G. M. *Photochem. Photobiol. Sci.* **2003**, *2*, 808.
(22) Morales-Cueto, R.; Esquivelzeta-Rabell, M.; Saucedo-Zugazagoitia, J.; Peon, J. *J. Phys. Chem. A* **2007**, *111*, 552.
(23) Zugazagoitia, J. S.; Almora-Díaz, C. X.; Peon, J. *J. Phys. Chem. A* **2008**, *112*, 358.
(24) Mohammed, O. F.; Vauthey, E. *J. Phys. Chem. A* **2008**, *112*, 3823.
(25) Crespo-Hernández, C. E.; Burdzinski, G.; Arce, R. *J. Phys. Chem. A* **2008**, *112*, 6313.
(26) Zugazagoitia, J. S.; Collado-Fregoso, E.; Plaza-Medina, E. F.; Peon, J. *J. Phys. Chem. A* **2009**, *113*, 805.
(27) Arce, R.; Pino, E. F.; Valle, C.; Ágreda, J. *J. Phys. Chem. A* **2008**, *112*, 10294.
(28) Il'ichev, Y. V. *J. Phys. Chem. A* **2003**, *107*, 10159.
(29) Naumov, P.; Sakurai, K.; Ishikawa, T.; Takahashi, J.; Koshihara, S.; Ohashi, Y. *J. Phys. Chem. A* **2005**, *109*, 7264.
(30) Leznoff, C. C.; Hayward, R. J. *Can. J. Chem.* **1971**, *49*, 3596.
(31) Mitsudo, T.; Fischetti, W.; Heck, R. F. *J. Org. Chem.* **1984**, *49*, 1640.
(32) Johnson, I. D.; Thomas, E. W.; Cundall, R. B. *J. Chem. Soc., Faraday Trans. 2* **1985**, *81*, 1303.
(33) Melhuish, W. H. *J. Phys. Chem.* **1961**, *65*, 229.
(34) *SMART Version 5.625*, Bruker AXS, Madison, WI. *SAINTPLUS Version 6.22*, Bruker AXS, Madison, WI. Sheldrick, G. M. *SADABS*, Program for scaling and correction of area, detector data, University of Göttingen, Germany, 1996.
(35) Altomare, A.; Cascarano, G.; Giacovazzo, C.; Guagliardi, A.; Brula, M. C.; Polidori, G.; Camalli, M. *J. Appl. Crystallogr.* **1994**, *27*, 435.
(36) Sheldrick, G. M., *SHELXTL Version 6.12*, Bruker AXS, Madison, WI, 2000.
(37) Frisch, M. J.; et al. *Gaussian 03, Revision C.02*; Gaussian, Inc.: Wallingford, CT, 2004.
(38) Mϕller, C.; Plesset, M. S. *Phys. Rev.* **1934**, *46*, 618.
(39) Lee, C.; Yang, W.; Parr, R. G. *Phys. Rev. B* **1988**, *37*, 785.
(40) Becke, A. D. *J. Chem. Phys.* **1993**, *98*, 5648.
(41) Foresman, J. B.; Head-Gordon, M.; Pople, J. A.; Frisch, M. J. *J. Phys. Chem.* **1992**, *96*, 135.
(42) Head-Gordon, M.; Rico, R. J.; Oumi, M.; Lee, T. J. *Chem. Phys. Lett.* **1994**, *219*, 21.
(43) Stratmann, R. E.; Scuseria, G. E.; Frisch, M. J. *J. Chem. Phys.* **1998**, *109*, 8218.
(44) Cundall, R. B.; Johnson, I.; Jones, M. W.; Thomas, E. W.; Munro, I. H. *Chem. Phys. Lett.* **1979**, *64*, 39.
(45) Onsager, L. *J. Am. Chem. Soc.* **1936**, *58*, 1486.
(46) Suppan, P. *J. Photochem. Photobiol., A* **1990**, *50*, 293.
(47) Banerji, N.; Angulo, G.; Barabanov, I.; Vauthey, E. *J. Phys. Chem. A* **2008**, *112*, 9665.
(48) Gierschner, J.; Mack, H.-G.; Lüer, L.; Oelkrug, D. *J. Chem. Phys.* **2002**, *116*, 8596.
(49) Lin-Vien, D.; Colthup, N. B.; Fateley, W. G.; Grasselli, J. G. *The Handbook of Infrared and Raman Characteristic Frequencies of Organic Molecules*; Academic Press: San Diego, CA, 1991.
(50) Kohler, B. E. *Chem. Rev.* **1993**, *93*, 41.
(51) For actual solution, we should also consider the presence of s-cis-s-trans isomers around the single bonds of the triene.[15,52] However, only all s-trans isomer was taken into account in the present case to avoid calculations that are too complex.
(52) Bunker, C. E.; Lytle, C. A.; Rollins, H. W.; Sun, Y.-P. *J. Phys. Chem. A* **1997**, *101*, 3214.
(53) Desiraju, G. R.; Steiner, T. *The Weak Hydrogen Bond in Structural Chemistry and Biology*; Oxford University Press: Oxford, 1999.
(54) Desiraju, G. R. *Chem. Commun.* **2005**, 2995.
(55) Ortí, E.; Viruela, P. M.; Viruela, R.; Effenberger, F.; Hernández, V.; Navarrete, J. T. L. *J. Phys. Chem. A* **2005**, *109*, 8724.
(56) Meng, S.; Ma, J. *J. Phys. Chem. B* **2008**, *112*, 4313.
(57) Šolc, R.; Lukeš, V.; Klein, E.; Griesser, M.; Kelterer, A.-M. *J. Phys. Chem. A* **2008**, *112*, 10931.
(58) Yang, S.; Kertesz, M. *J. Phys. Chem. A* **2006**, *110*, 9771.
(59) Sonoda, Y.; Tsuzuki, S.; Tamaoki, N.; Goto, M. *Acta Crystallogr.* **2007**, *C63*, o196.
(60) Wu, C.; Tretiak, S.; Chernyak, V. Y. *Chem. Phys. Lett.* **2007**, *433*, 305.
(61) Jacquemin, D.; Perpète, E. A.; Ciofini, I.; Adamo, C. *Chem. Phys. Lett.* **2005**, *405*, 376.
(62) Tsuzuki, S.; Tanabe, K.; Osawa, E. *J. Phys. Chem.* **1990**, *94*, 6175.
(63) Head-Gordon, M.; Pople, J. A. *Chem. Phys. Lett.* **1990**, *173*, 585.
(64) Takezaki, M.; Hirota, N.; Terazima, M.; Sato, H.; Nakajima, T.; Kato, S. *J. Phys. Chem. A* **1997**, *101*, 5190.
(65) Hsu, C.-P.; Hirata, S.; Head-Gordon, M. *J. Phys. Chem. A* **2001**, *105*, 451.
(66) Ma, H.; Liu, C.; Jiang, Y. *J. Chem. Phys.* **2005**, *123*, 084303.
(67) Grimme, S.; Neese, F. *J. Chem. Phys.* **2007**, *127*, 154116.
(68) Scheiner, S. *J. Phys. Chem. A* **2000**, *104*, 5898.
(69) Sobolewski, A. L.; Domcke, W. *J. Phys. Chem. A* **2007**, *111*, 11725.
(70) Klessinger, M.; Michl, J. *Excited States and Photochemistry of Organic Molecules*; VCH Publishers, Inc.: New York, 1995; sections 1-3 and 5-2.
(71) Van Hutten, P. F.; Krasnikov, V. V.; Hadziioannou, G. *Acc. Chem. Res.* **1999**, *32*, 257.
(72) Sonoda, Y.; Kawanishi, Y.; Goto, M. *Acta Crystallogr.* **2005**, *E61*, o1200.
(73) Sluch, M. I.; Godt, A.; Bunz, U. H. F.; Berg, M. A. *J. Am. Chem. Soc.* **2001**, *123*, 6447.
(74) Li, N.; Jia, K.; Wang, S.; Xia, A. *J. Phys. Chem. A* **2007**, *111*, 9393.
(75) Grabowski, Z. R.; Rotkiewicz, K.; Rettig, W. *Chem. Rev.* **2003**, *103*, 3899.
(76) Demeter, A.; Zachariasse, K. A. *Chem. Phys. Lett.* **2003**, *380*, 699.
(77) Druzhinin, S. I.; Dubbaka, S. R.; Knochel, P.; Kovalenko, S. A.; Mayer, P.; Senyushkina, T.; Zachariasse, K. A. *J. Phys. Chem. A* **2008**, *112*, 2749.
(78) Singh, A. K.; Darshi, M.; Kanvah, S. *J. Phys. Chem. A* **2000**, *104*, 464.

JP907441P